J. Fluid Mech. (1990), *vol.* 215, *pp.* 639–657
Printed in Great Britain

A structural turbulence model for triple products of velocity and scalar

By Y. NAGANO AND M. TAGAWA

Department of Mechanical Engineering, Nagoya Institute of Technology, Gokiso-cho, Showa-ku, Nagoya 466, Japan

(Received 29 May 1989 and in revised form 8 December 1989)

The statistical characteristics of third-order moments (triple products) of velocity and scalar have been investigated from both experimental and theoretical points of view. The third-order moments have a highly intermittent nature and are dominated by coherent motions in shear-generated turbulence. Using a previously developed statistical method (Nagano & Tagawa 1988), the similarity between the Reynolds stress and scalar flux transport was analysed. On the basis of the experimental results, we have developed an entirely new approach to the modelling of triple products, and constructed a 'structural' turbulence model for triple velocity and scalar products. This model has a simple form and universal applicability, and its effectiveness has been tested by application to various types of flow.

1. Introduction

As the most advanced mathematical models of turbulence, the Reynolds-stress and scalar-flux equation models (e.g. Lumley 1978) have often been used to analyse transport phenomena in various types of turbulent flows. However, despite the widespread expectation that these models ought to be accurate, their record of success thus far does not appear to justify this opinion. In a previous study (Nagano & Tagawa 1988), we have shown that one important cause is the breakdown of the conventional models for triple products of velocity and scalar (third-order moments). To resolve the underlying problems involved in the conventional gradient-type diffusion modelling of triple products, we investigated the statistical characteristics of third-order moments from both experimental and theoretical points of view and reached the following conclusions (Nagano & Tagawa 1988): (i) the statistical characteristics of third-order moments such as probability distributions and internal structures are essentially dominated by the dynamical flow structures; hence, (ii) for appropriately modelling the turbulent diffusion terms in the second-order closure models, we need to develop a new model based not on the unreal assumption of gradient-type diffusion but on the physical behaviour of triple products.

Representative existing models for triple products are those proposed by Daly & Harlow (1970), Hanjalić & Launder (1972*b*) and Cormack, Leal & Seinfeld (1978) for a velocity field, and by Donaldson, Sullivan & Rosenbaum (1972), Deardorff (1973), Owen (1973) and Wyngaard & Coté (1974) for a scalar field. These models are frequently used, mainly because of the formal simplicity of their equations. Key points of these models, however, are based on a somewhat intuitive assumption of gradient-type diffusion. Hence, their use sometimes leads to incorrect results even in a qualitative sense (see Nagano & Tagawa 1988).

Chandrsuda & Bradshaw (1981) investigated the detailed turbulence structure of

a reattaching mixing layer over a backward-facing step and pointed out that any calculation method intended to deal with reattaching flows should include a fairly sophisticated model for triple products, preferably based on the triple-product transport equation. Modelling of triple products based on their transport equations has been done by Hanjalić & Launder (1972*b*), Deardorff (1978), André *et al.* (1979), Dekeyser & Launder (1985), Amano, Goel & Chai (1988) and Amano & Chai (1988). Hanjalić & Launder (1972*b*) derived a simple model through omission or modelling of each term in a triple-product transport equation. As stated above, the final form of this model resulted in a gradient-type diffusion representation, and thus its applicability is limited. On the other hand, André *et al.* (1979) and Dekeyser & Launder (1985) modelled all the terms which appear in the transport equations of triple products of velocity and scalar so as to make the models more universal. However, although the modelled equations are numerous and complicated, application to an asymmetric heated jet (Dekeyser & Launder 1985) results in little improvement in the calculated results. Amano *et al.* (1988) and Amano & Chai (1988) also modelled the transport equations of triple products in a manner similar to Dekeyser & Launder (1985), and calculated the backward-facing step flows reported by Chandrsuda & Bradshaw (1981) and Driver & Seegmiller (1985). Improved results can be seen in the predictions, but the systems of modelled equations seem also too numerous and complex to readily incorporate in the second-order closure modelling.

In the present study, we aim at providing a new representation of triple velocity and scalar products. First, we apply the previously developed statistical method (Nagano & Tagawa 1988) to an analysis of the measurement of wall turbulence with a passive scalar to understand the further details of statistical characteristics of triple products. Next, we construct a 'structural model' for triple products from an entirely new point of view on the basis of the experimental facts. The performance of the proposed model is tested by applications to various types of flows.

2. Experimental facility and data acquisition

The experimental set-up used for the present study is the same as that of Nagano & Tagawa (1988). The experiment was performed in an air flow in a 45.68 mm ID tube heated to a uniform wall temperature of 100 °C. Both velocity and scalar (thermal) fields were fully developed at a measurement location. The centreline velocity and temperature were 17.2 m/s and 41.2 °C. Reynolds numbers based on bulk velocity and pipe diameter, and on centreline velocity and momentum thickness are 40000 and 1032, respectively. Fluctuations of velocity components, u (streamwise) and v (normal), and scalar (temperature), θ, were simultaneously measured with a specially devised three-wire probe comprised of two hot and one cold wires (Nagano & Tagawa 1988). For each set of u-, v- and θ-fluctuations, all data were digitized with a 12-bit analog-to-digital converter at a sampling frequency of 32 kHz. There were 65536 pieces of data per measurement. Measurement uncertainty was estimated in conformity with the ANSI/ASME standard, PTC 19.1-1985 (1986), and with Bendat & Piersol (1971). The statistical analysis of the data was performed on a FACOM M-780/20 computer system.

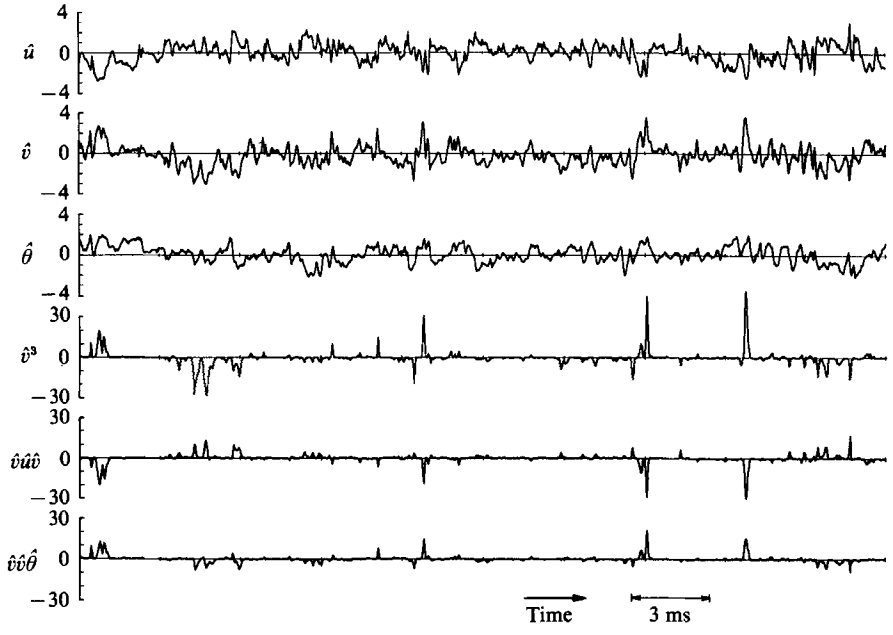

FIGURE 1. Simultaneous signal traces of third-order moments $\hat{v}^3$, $\hat{v}\hat{u}\hat{v}$ and $\hat{v}\hat{v}\hat{\theta}$ ($y^+ = 37.1$).

3. Detailed statistical characteristics of third-order moments

3.1. *Instantaneous signals of third-order moments*

To describe the production mechanism of triple products, first we investigated the simultaneous signal traces of third-order moments. Figure 1 shows sample instantaneous signals of v^3, vuv and $vv\theta$ together with u-, v- and θ-fluctuations, which are recorded at $y^+ = 37.1$ where the time-averaged absolute values of triple products become nearly maximum (Nagano & Tagawa 1988). In this figure and also in what follows, a circumflex denotes the normalization by the respective r.m.s. value. Obviously, all third-order moments fluctuate very intermittently and almost symmetrically about zero except for infrequent, very large-amplitude fluctuations. These features are quite different from those of the second-order moments such as Reynolds shear stress, uv, and scalar flux, $v\theta$ (Nagano & Hishida 1990). Large-amplitude fluctuations of triple products are associated only with the fluid motions categorized as the second- and fourth-quadrant events in the (u,v)-plane. These motions are termed the Q2- and Q4-motions, respectively, and reflect the very important motions of ejections and sweeps, which are known as the basic flow modules of coherent structures in wall turbulence. Just as the Q2- and Q4-motions contribute greatly to the production of $\overline{uv}$ and $\overline{v\theta}$, so these motions can be regarded as the main contributors to thc production process of triple products as observed in figure 1. Very large-amplitude fluctuations of v^3, vuv and $vv\theta$ are slightly skewed to the positive, negative and positive sides, respectively, and this delicate imbalance determines the net values of triple products of velocity and scalar.

3.2. *Skewness and flatness factors of third-order moments*

The previous analysis (Nagano & Tagawa 1988) revealed the general characteristics of probability density functions (p.d.f.s) of third-order moments. Here, to determine

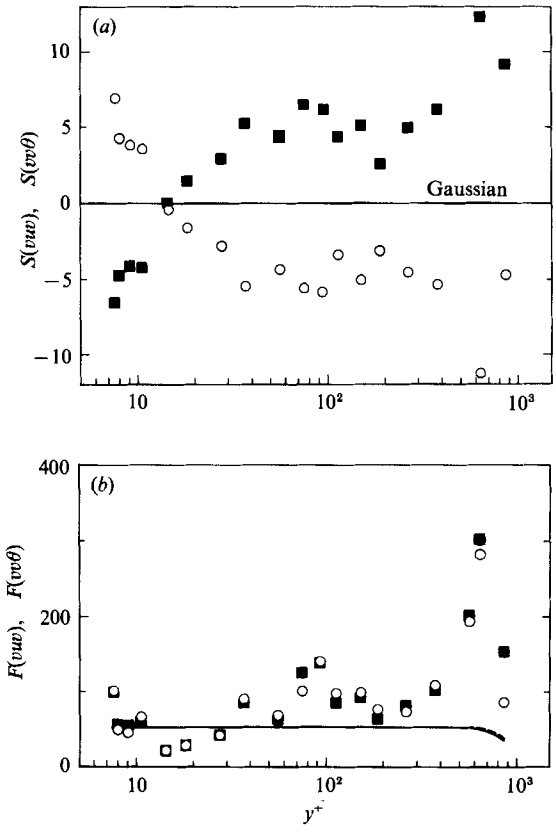

FIGURE 2. Skewness and flatness factors of vuv and $vv\theta$. (a) Skewness factors. Experiments: ○, $S(vuv)$; ■, $S(vv\theta)$. Measurement uncertainty at 95% coverage: ±18%. (b) Flatness factors. Experiments: ○, $F(vuv)$; ■, $F(vv\theta)$. Gaussian values calculated from (4): ——, $F(vuv)$; – – –, $F(vv\theta)$. Measurement uncertainty at 95% coverage: ±33%.

these features quantitatively, we investigate the skewness and flatness factors of third-order moments. The skewness and flatness factors, $S(x)$ and $F(x)$, are respectively defined by

$$S(x) = \overline{(x-\bar{x})^3}/[\overline{(x-\bar{x})^2}]^{\frac{3}{2}}, \tag{1}$$

$$F(x) = \overline{(x-\bar{x})^4}/[\overline{(x-\bar{x})^2}]^2, \tag{2}$$

where an overbar denotes an expected value or time average. If a joint p.d.f. $P(u, v, \theta)$ is Gaussian, the skewness factor of any third-order moment is consistently zero. On the other hand, using the Isserlis' rule for Gaussian fields (Monin & Yaglom 1971), we can write the Gaussian flatness factors for $x = \chi_1^3$, $\chi_1\chi_2^2$ and $\chi_1\chi_2\chi_3$ as follows:

$$F(\chi_1^3) = 10395/15^2 = 46.2, \tag{3}$$

$$F(\chi_1\chi_2^2) = [315 + 5040R_{12}^2 + 5040R_{12}^4]/(3+12R_{12}^2)^2, \tag{4}$$

$$\left.\begin{aligned} F(\chi_1\chi_2\chi_3) &= [27 + 216a_1(1+2a_1) + 576a_2(3+2a_1+3a_2) - 360a_3]/(1+2a_1+8a_2)^2, \\ a_1 &= R_{12}^2 + R_{13}^2 + R_{23}^2, \quad a_2 = R_{12}R_{13}R_{23}, \quad a_3 = R_{12}^4 + R_{13}^4 + R_{23}^4, \end{aligned}\right\} \tag{5}$$

where R_{12}, R_{13} and R_{23} are the correlation coefficients defined as $R_{12} = \overline{\hat{\chi}_1\hat{\chi}_2}$, $R_{13} = \overline{\hat{\chi}_1\hat{\chi}_3}$ and $R_{23} = \overline{\hat{\chi}_2\hat{\chi}_3}$, respectively.

It is the third-order moments $\overline{vuv}$ and $\overline{vv\theta}$ that play an important role in the Reynolds-stress and scalar-flux equation modelling. Figure 2(*a*, *b*) shows the measurements of skewness and flatness factors of vuv and $vv\theta$, respectively. As seen in figure 2(*a*), $S(vuv)$ and $S(vv\theta)$ behave like a reflected image about zero. Their absolute values are nearly constant at 5 in the log-law region, but very near the wall ($y^+ < 30$), they change very steeply. These distinct features are mainly the consequence of coherent motions in wall turbulence. The Q4-motions ($u > 0$, $v < 0$) dominate over the Q2-motions ($u < 0, v > 0$) near the wall ($y^+ < 15$) and vice versa in the region away from the wall; hence, $S(vuv)$ turns from negative to positive as the wall is approached. Similar characteristics can also be seen in $S(vv\theta)$. Thus, because the Q4-motions with $\theta < 0$ and Q2-motions with $\theta > 0$ are prominent in a heated wall turbulence (Nagano & Tagawa 1988), $S(vv\theta)$ becomes negative in the region $y^+ < 15$ and positive further out. Consequently, though with opposite signs, $S(vv\theta)$ and $S(vuv)$ become very similar.

Figure 2(*b*) shows the flatness factors of vuv and $vv\theta$, compared to the calculations from (4). Usually, high flatness factors correspond to intermittent signals. As shown in figure 2(*b*), $F(vuv)$ and $F(vv\theta)$ are very high, amounting to as high as 80 in the log-law region, which further corroborates the fact that the third-order moments possess a very highly intermittent nature. Note that flatness factors of u, v and θ are about 3 in the same region. Also important is the fact that the distributions of $F(vuv)$ and $F(vv\theta)$ are nearly identical over the entire flow zone. This fact together with a close similarity in skewness suggests that the triple products vuv and $vv\theta$ are governed by identical physical laws.

The flatness factors, $F(vuv)$ and $F(vv\theta)$, have their minima at about $y^+ = 15$ where the corresponding skewness factors become zero. This is a characteristic common to other lower-order moments $F(u)$, $F(v)$, $F(\theta)$, $F(uv)$, $F(u\theta)$ and $F(v\theta)$ (Zarić 1979; Durst, Jovanovic & Kanevce 1987). It should also be noted here that the calculated Gaussian values from (4) are almost constant over the entire region, agreement with the experiments being seen only in a part of the log-law region.

From these results, we may conclude that the triple products vuv and $vv\theta$ have similar statistical characteristics different from the Gaussian, which are under the strong influence of coherent structures.

3.3. *Fractional contributions of coherent motions to triple products of velocity and scalar*

Coherent structures in turbulence can be described appropriately with fluid motions classified in the (u, v)-plane. The fractional contributions of different quadrant motions to $\overline{vuv}$ and $\overline{vv\theta}$ are shown in figure 3(*a*, *b*), respectively. A prime denotes the normalization of velocity and scalar (temperature) by the friction velocity and friction temperature, respectively. As is apparent from figure 3, the turbulent transport of $\overline{uv}$ and $\overline{v\theta}$, i.e. $\overline{vuv}$ and $\overline{vv\theta}$, are dominated almost completely by the Q2- ($i = 2$) and Q4-motions ($i = 4$), and hence the net values are determined by the disparity in contributions between these two types of motions. The interactive fluid motions classified into the first- and third-quadrants in the (u, v)-plane, i.e. Q1- and Q3-motions, contribute very little to the net values because both contributions are quite small in absolute value and the signs cancel out. In short, the triple products of velocity and scalar are determined by the dynamic fluid motions such as the ejections (Q2-motions) and sweeps (Q4-motions). And this may explain why the triple products could not be described adequately by a conventional static model such as gradient-type diffusion of second-order moments.

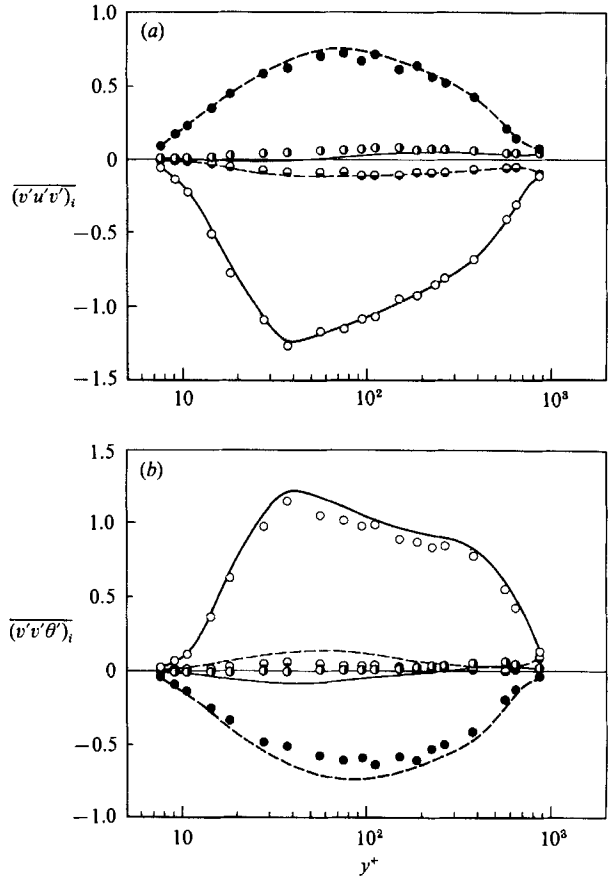

FIGURE 3. Fractional contributions of different quadrant motions to the third-order moments $\overline{vuv}$ and $\overline{vv\theta}$. (*a*) $\overline{(vuv)_i}$. Experiments: ◑, $i = 1$; ○, $i = 2$; ◒, $i = 3$; ●, $i = 4$. Calculations from (21): ——, $i = 1$; ——, $i = 2$; – – –, $i = 3$; – – –, $i = 4$. (*b*) $\overline{(vv\theta)_i}$. Experiments: ◑, $i = 1$; ○, $i = 2$; ◒, $i = 3$; ●, $i = 4$. Calculations from (22): ——, $i = 1$; ——, $i = 2$; – – –, $i = 3$; – – –, $i = 4$.

Now, to describe theoretically the above-mentioned behaviour of triple products, we use the previously developed statistical theory for non-Gaussian fields (Nagano & Tagawa 1988) outlined below.

With $\hat{u}$, $\hat{v}$ and $\hat{\theta}$ as random variables, the characteristic function ψ, which is the Fourier transform of the p.d.f., can be written as

$$\psi(\xi,\eta,\zeta) = \iiint_{-\infty}^{\infty} P(\hat{u},\hat{v},\hat{\theta}) \exp\{\mathrm{i}(\hat{u}\xi+\hat{v}\eta+\hat{\theta}\zeta)\}\,\mathrm{d}\hat{u}\,\mathrm{d}\hat{v}\,\mathrm{d}\hat{\theta}. \tag{6}$$

If a proper form is given to the characteristic function ψ defined by (6), the three-dimensional joint p.d.f. $P(\hat{u},\hat{v},\hat{\theta})$ can be obtained by executing the inverse Fourier transform of ψ. Hence, we describe the characteristic function ψ in terms of a cumulant k_{pqr}, which is defined as

$$\left.\frac{\partial^K \ln\psi(\xi,\eta,\zeta)}{\partial\xi^p\,\partial\eta^q\,\partial\zeta^r}\right|_{\xi=\eta=\zeta=0} = \mathrm{i}^K k_{pqr}, \tag{7}$$

where $K = p+q+r$.

Integration of (7) leads to

$$\psi(\xi,\eta,\zeta)=\exp\Big(\sum_{p,q,r=0}^{\infty}\frac{\mathrm{i}^K}{p!\,q!\,r!}k_{pqr}\,\xi^p\,\eta^q\,\zeta^r\Big). \tag{8}$$

On the other hand, the definition of a moment m_{pqr} is

$$m_{pqr}=\overline{\hat{u}^p\,\hat{v}^q\,\hat{\theta}^r}=\iiint_{-\infty}^{\infty}\hat{u}^p\,\hat{v}^q\,\hat{\theta}^r\,P(\hat{u},\hat{v},\hat{\theta})\,\mathrm{d}\hat{u}\,\mathrm{d}\hat{v}\,\mathrm{d}\hat{\theta}. \tag{9}$$

Equations (6) and (9) give

$$\left.\frac{\partial^K\psi(\xi,\eta,\zeta)}{\partial\xi^p\,\partial\eta^q\,\partial\zeta^r}\right|_{\xi=\eta=\zeta=0}=\mathrm{i}^K\,m_{pqr}. \tag{10}$$

Thus, from (7) and (10), we obtain the following relations between m_{pqr} and k_{pqr}:

$$\left.\begin{aligned}&m_{000}=1,\,k_{000}=0 \quad \text{for } K=0;\\ &m_{pqr}=k_{pqr} \qquad\quad \text{for } 1\leqslant K\leqslant 3;\end{aligned}\right\}$$

and

$$\left.\begin{aligned}&m_{400}=k_{400}+3,\quad m_{040}=k_{040}+3,\quad m_{004}=k_{004}+3,\\ &m_{310}=k_{310}+3m_{110},\quad m_{301}=k_{301}+3m_{101},\ldots,\\ &m_{013}=k_{013}+3m_{011},\\ &m_{220}=k_{220}+2(m_{110})^2+1,\ldots,\\ &m_{112}=k_{112}+2m_{101}\,m_{011}+m_{110},\end{aligned}\right\}\ \text{for } K=4. \tag{11}$$

Using (11), we can write (8) as

$$\psi(\xi,\eta,\zeta)=\exp\Big\{-\tfrac{1}{2}(\xi^2+\eta^2+\zeta^2+2R_{uv}\,\xi\eta+2R_{u\theta}\,\xi\zeta+2R_{v\theta}\,\eta\zeta)+\sum_{K\geqslant 3}^{\infty}\frac{\mathrm{i}^K}{p!\,q!\,r!}k_{pqr}\,\xi^p\,\eta^q\,\zeta^r\Big\}, \tag{12}$$

where $k_{110}=m_{110}=\overline{\hat{u}\hat{v}}=R_{uv}$, $k_{101}=R_{u\theta}$ and $k_{011}=R_{v\theta}$. Obviously, (12) can be rewritten as

$$\psi(\xi,\eta,\zeta)=\exp\{-\tfrac{1}{2}(\xi^2+\eta^2+\zeta^2)\}\sum_{p,q,r=0}^{\infty}C_{pqr}\,\mathrm{i}^K\,\xi^p\,\eta^q\,\zeta^r, \tag{13}$$

where C_{pqr} is the coefficients in the power-series expansion of (12).

Substituting the characteristic function (13) into (6) and performing the inverse Fourier transform, we obtain the following general representation for $P(\hat{u},\hat{v},\hat{\theta})$:

$$\begin{aligned}P(\hat{u},\hat{v},\hat{\theta})&=\frac{1}{(2\pi)^3}\iiint_{-\infty}^{\infty}\psi(\xi,\eta,\zeta)\exp\{-\mathrm{i}(\hat{u}\xi+\hat{v}\eta+\hat{\theta}\zeta)\}\,\mathrm{d}\xi\,\mathrm{d}\eta\,\mathrm{d}\zeta\\ &=\frac{1}{(2\pi)^{\frac{3}{2}}}\sum_{p,q,r=0}^{\infty}C_{pqr}\,H_p(\hat{u})\,H_q(\hat{v})\,H_r(\hat{\theta})\exp\{-\tfrac{1}{2}(\hat{u}^2+\hat{v}^2+\hat{\theta}^2)\},\end{aligned} \tag{14}$$

where $H_n(\chi)$ is an Hermite polynomial defined by

$$H_n(\chi)=(-1)^n\exp(\tfrac{1}{2}\chi^2)\frac{\mathrm{d}^n}{\mathrm{d}\chi^n}\exp(-\tfrac{1}{2}\chi^2). \tag{15}$$

The subsequent analysis has been made for $K \leqslant 4$ to avoid cumbersome calculations (Nagano & Tagawa 1988).

Calculating C_{pqr} from (12) and (13) yields

$$\left.\begin{aligned}
&C_{000}=1, \quad C_{100}=C_{010}=C_{001}=0, \quad C_{200}=C_{020}=C_{002}=0,\\
&C_{110}=k_{110}=\overline{\hat{u}\hat{v}}=R_{uv}, \quad C_{101}=k_{101}=\overline{\hat{u}\hat{\theta}}=R_{u\theta}, \quad C_{011}=k_{011}=\overline{\hat{v}\hat{\theta}}=R_{v\theta},\\
&C_{300}=\tfrac{1}{6}k_{300}=\tfrac{1}{6}\overline{\hat{u}^3}=\tfrac{1}{6}S(u), \quad C_{030}=\tfrac{1}{6}S(v), \quad C_{003}=\tfrac{1}{6}S(\theta),\\
&C_{210}=\tfrac{1}{2}k_{210}=\tfrac{1}{2}\overline{\hat{u}^2\hat{v}}, \ldots, \quad C_{012}=\tfrac{1}{2}k_{012}=\tfrac{1}{2}\overline{\hat{v}\hat{\theta}^2}, \quad C_{111}=k_{111}=\overline{\hat{u}\hat{v}\hat{\theta}},\\
&C_{400}=\tfrac{1}{24}k_{400}, \ldots, \quad C_{310}=\tfrac{1}{6}k_{310}, \ldots, \quad C_{013}=\tfrac{1}{6}k_{013},\\
&C_{220}=\tfrac{1}{4}(k_{220}+2k_{110}^2), \ldots, \quad C_{112}=\tfrac{1}{2}(k_{112}+2k_{101}k_{011}).
\end{aligned}\right\} \tag{16}$$

The coefficients listed above are determined from the measured correlations up to the fourth order (see (11)).

Next, to represent the fractional contributions to the moment $\overline{u^l v^m \theta^n}$ from Qi-motions classified in the (u,v)-plane, we calculate $\overline{(u^l v^m \theta^n)_i}$ separately in each quadrant of the (u,v)-plane with (14):

$$\overline{(\hat{u}^l \hat{v}^m \hat{\theta}^n)_i} = \sigma_{u,i}^l \sigma_{v,i}^m \int_0^\infty \left[\int_0^\infty \left\{ \int_{-\infty}^\infty \hat{u}^l \hat{v}^m \hat{\theta}^n P(\sigma_{u,i}\hat{u}, \sigma_{v,i}\hat{v}, \hat{\theta}) \, \mathrm{d}\hat{\theta} \right\} \mathrm{d}\hat{v} \right] \mathrm{d}\hat{u}, \tag{17}$$

where $\sigma_{u,i}$ and $\sigma_{v,i}$ are sign functions which represent the signs of u and v of the ith quadrant in the (u,v)-plane:

$$\sigma_{u,i} = (1,-1,-1,1), \quad \sigma_{v,i} = (1,1,-1,-1). \tag{18}$$

For example, for $i=2$, we have $(\sigma_{u,i}, \sigma_{v,i}) = (-1,1)$. Substitution of (14)–(16) into (17) yields

$$\overline{(\hat{u}^l \hat{v}^m \hat{\theta}^n)_i} = \frac{2}{(2\pi)^{\frac{3}{2}}} \sum_{\substack{p,q,r=0 \\ n+r=\text{even}}}^{K \leqslant 4} \sigma_{u,i}^{l+p} \sigma_{v,i}^{m+q} C_{pqr} B_{l,p} B_{m,q} B_{n,r}, \tag{19}$$

where $B_{j,k}$ is defined as

$$B_{j,k} = \int_0^\infty \chi^j H_k(\chi) \exp(-\tfrac{1}{2}\chi^2) \, \mathrm{d}\chi. \tag{20}$$

For $\overline{(vuv)_i}$ (with $l=1$, $m=2$, $n=0$) and $\overline{(vv\theta)_i}$ (with $l=0$, $m=2$, $n=1$), equation (19) is reduced to

$$\begin{aligned}
\overline{(\hat{v}\hat{u}\hat{v})_i} = {} & \tfrac{1}{4}\overline{\hat{v}\hat{u}\hat{v}} + \sigma_{u,i} \frac{1}{2(2\pi)^{\frac{1}{2}}} (1 + 2C_{220} - C_{400}) \\
& + \sigma_{v,i} \frac{1}{(2\pi)^{\frac{1}{2}}} (C_{110} + C_{130}) + \sigma_{u,i}\sigma_{v,i} \frac{1}{\pi} (C_{210} + C_{030}),
\end{aligned} \tag{21}$$

and

$$\begin{aligned}
\overline{(\hat{v}\hat{v}\hat{\theta})_i} = {} & \tfrac{1}{4}\overline{\hat{v}\hat{v}\hat{\theta}} + \sigma_{u,i} \frac{1}{2(2\pi)^{\frac{1}{2}}} (C_{101} + 2C_{121} - C_{301}) \\
& + \sigma_{v,i} \frac{1}{(2\pi)^{\frac{1}{2}}} (C_{011} + C_{031}) + \sigma_{u,i}\sigma_{v,i} \frac{1}{\pi} C_{111}.
\end{aligned} \tag{22}$$

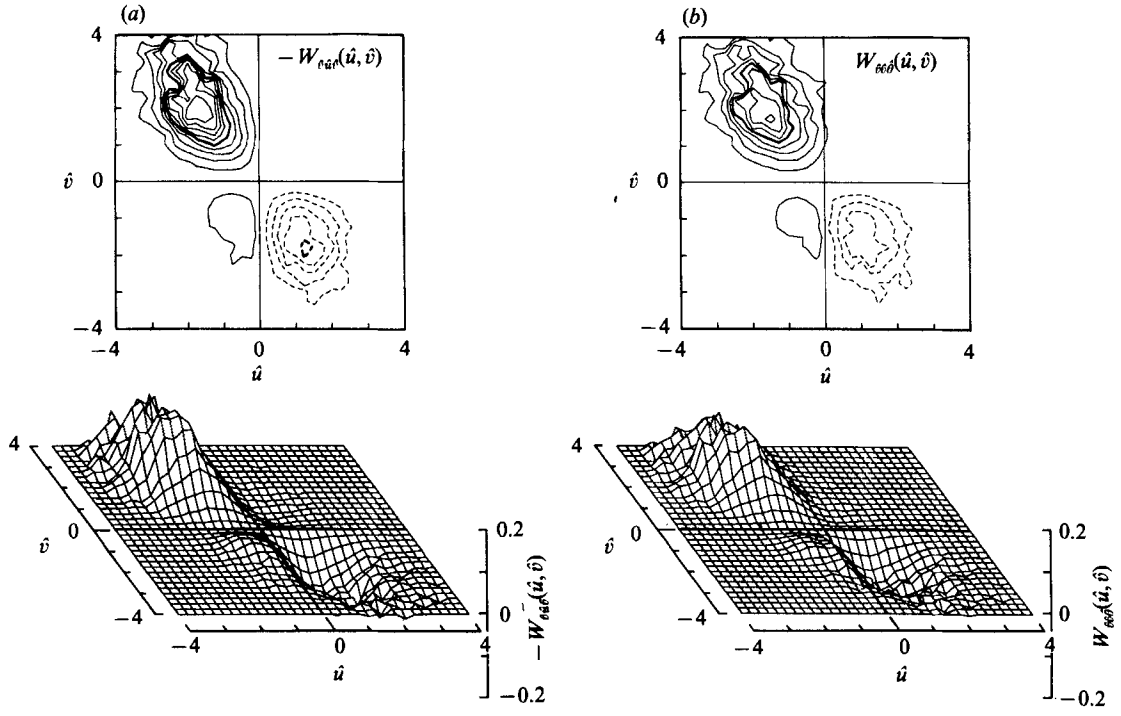

FIGURE 4. Experimental distributions of the weighted p.d.f.s of $-\hat{v}\hat{u}\hat{v}$ and $\hat{v}\hat{v}\hat{\theta}$ ($y^+ = 37.1$). (*a*) $-W_{\hat{v}\hat{u}\hat{v}}$; (*b*) $W_{\hat{v}\hat{v}\hat{\theta}}$.

Curves in figure 3 represent the theoretical predictions from (21) and (22), and it can be seen that they reproduce the above-mentioned dynamic behaviour of the third-order moments reasonably well. On the other hand, if a Gaussian distribution is assumed for $P(\hat{u},\hat{v},\hat{\theta})$, the fractional contributions of Q2- and Q4-motions to any third-order moment become equal, though with opposite signs. Hence, the foregoing important characteristics of third-order moments cannot be fully described.

3.4. *Weighted p.d.f.s of vuv and vvθ in the* (u,v)*-plane*

The analysis of fractional contributions in the (u,v)-plane alone is not sufficient to ascertain the detailed correspondence between fluid motions and production processes of triple products. Hence, we investigate the weighted p.d.f., $W_x(\hat{u},\hat{v})$, of triple products $\overline{vuv}$ and $\overline{vv\theta}$ in the (u,v)-plane (Nagano & Tagawa 1988):

$$W_x(\hat{u},\hat{v}) = \int_{-\infty}^{\infty} x P(\hat{u},\hat{v},\hat{\theta})\,\mathrm{d}\hat{\theta}, \quad x = \hat{u}^l \hat{v}^m \hat{\theta}^n. \tag{23}$$

This function provides a powerful tool to see which fluid motion makes a large contribution to the production of the triple products. The integrated value of $W_x(\hat{u},\hat{v})$ in each quadrant becomes the fractional contribution $\overline{(x)}_i$, and integration over the whole (u,v)-plane reduces to the conventional time-averaged value $\bar{x}$.

The experimental distributions of W_x for $x = -\hat{v}\hat{u}\hat{v}$ and $\hat{v}\hat{v}\hat{\theta}$ at $y^+ = 37.1$ are shown in figure 4(*a*, *b*), respectively. In the contour maps of figure 4, solid and broken lines respectively represent positive and negative values, and interval between successive contour lines is 0.02. There is a strong resemblance between these two figures, which

suggests that there exists a close similarity in the detailed generation process between $\overline{vuv}$ and $\overline{vv\theta}$, thus substantiating the results in §3.2. Furthermore, we can clearly see that the large-amplitude Q2-motions contribute significantly to $\overline{vuv}$ and $\overline{vv\theta}$. This fact accords with the results shown in figure 3.

4. Structural modelling of triple velocity and scalar products

4.1. *Structural turbulence model for triple products in velocity field*

As suggested from the statistical analysis in §3, the turbulent transport of second-order moments has a highly intermittent nature and is dominated almost completely by the coherent structures in a turbulent shear flow. Hence, we may utilize this experimental fact for modelling the triple products.

Considering the structural similarity which is common to shear-generated turbulence (Lee, Kim & Moin 1987; Moin 1990), we can expect wide applicability of the foregoing quadrant analysis. The Q2- and Q4-motions, which correspond to the ejections and sweeps, are found to play a key role in determining the internal structures of turbulence statistics in wall turbulence. On the other hand, the Q1- and Q3-motions are important in pattern recognition of the coherent structures in wall turbulence (Nagano & Hishida 1990). However, as shown in figure 3, we may discard the contributions of Q1- and Q3-motions to the net values of the triple products. This can be described by the following equations for $\overline{vuv}$ and $\overline{vu^2}$:

$$\overline{vuv} \approx \overline{(vuv)}_{t-2} + \overline{(vuv)}_{t-4}, \tag{24}$$

$$\overline{vu^2} \approx \overline{(vu^2)}_{t-2} + \overline{(vu^2)}_{t-4}. \tag{25}$$

The calculations from (21), as shown in figure 3(*a*), agree well with the experiment. Hence, substituting (21) into (24), we may model the triple product based on the physical behaviour. The result is

$$\begin{aligned}\overline{\hat{v}\hat{u}\hat{v}} &\approx \tfrac{1}{2}\overline{\hat{v}\hat{u}\hat{v}} - \frac{2}{\pi}(C_{210} + C_{030}) \\ &= \tfrac{1}{2}\overline{\hat{v}\hat{u}\hat{v}} - \frac{1}{\pi}[\overline{\hat{v}\hat{u}^2} + \tfrac{1}{3}S(v)].\end{aligned} \tag{26}$$

A similar calculation for (25) yields

$$\overline{\hat{v}\hat{u}^2} \approx \tfrac{1}{2}\overline{\hat{v}\hat{u}^2} - \frac{1}{\pi}[\overline{\hat{v}\hat{u}\hat{v}} + \tfrac{1}{3}S(u)], \tag{27}$$

where $S(\chi)$ is the skewness factor of a stochastic variable $\chi\,(=\overline{\hat{\chi}^3})$. From (26) and (27), $\overline{vuv}$ and $\overline{vu^2}$ can be represented with $S(u)$ and $S(v)$ as

$$\overline{\hat{v}\hat{u}\hat{v}} = C[S(u) + \sigma_{uv}\tfrac{1}{2}\pi S(v)], \tag{28}$$

$$\overline{\hat{v}\hat{u}^2} = C[\sigma_{uv}\tfrac{1}{2}\pi S(u) + S(v)], \tag{29}$$

$$C = \frac{1}{3[(\frac{1}{2}\pi)^2 - 1]}, \tag{30}$$

where σ_{uv} represents a sign function introduced to make a model independent of a coordinate system:

$$\sigma_x = \begin{cases} 1, & x \geqslant 0 \\ -1, & x < 0. \end{cases} \tag{31}$$

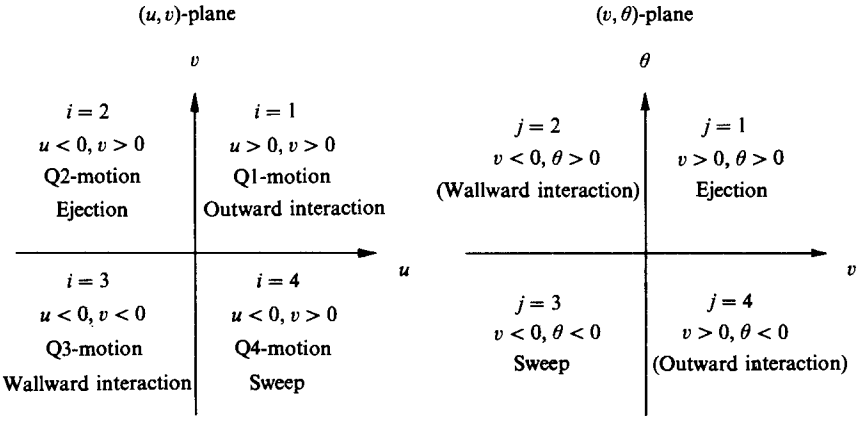

FIGURE 5. Correspondence between quadrant motions and events in the (v, θ)-plane.

For $\overline{vuv}$, $\sigma_{\overline{uv}}$ is equal to -1 because $x = \overline{uv} < 0$. We term the present model such as (28) or (29) a 'structural' model for a triple product, since it is constructed on the basis of the structure of turbulence. The usefulness of the present structural model is discussed in §6.

4.2. *Structural turbulence model for triple products in a scalar field*

We can also apply the theoretical approach of §4.1 to the modelling of triple products in a scalar field, $\overline{vv\theta}$, $\overline{v\theta^2}$, $\overline{vu\theta}$, etc. As with the triple products in a velocity field, those in a scalar field are also determined by the Q2- and Q4-motions (see figure 3*b*). In modelling $\overline{vv\theta}$ and $\overline{v\theta^2}$, however, the analysis in the (v, θ)-, instead of the (u, v)-plane makes the modelling much simpler, because we can use exactly the same procedure as in the modelling of $\overline{vuv}$ and $\overline{vu^2}$.

In heated wall turbulence, since the Q2-motions ($v > 0$) with $\theta > 0$ and Q4-motions ($v < 0$) with $\theta < 0$ are most probable (Nagano & Tagawa 1988), the ejections and sweeps are classified approximately into the first and third quadrants in the (v, θ)-plane. While the quadrants corresponding to the Q1- and Q3-motions cannot be specified clearly in the (v, θ)-plane, we may catalogue the relation between the (u, v)-plane and (v, θ)-plane as presented in figure 5. In the following, a quadrant in the (u, v)-plane and that in the (v, θ)-plane are denoted by the suffixes i and j, respectively.

Figure 6 (*a*, *b*), respectively, shows the measurements of $\overline{(vv\theta)_j}$ and $\overline{(v\theta^2)_j}$, compared with the theoretical predictions from the following equation, which is derived using the same procedure as for (17):

$$\overline{(\hat{u}^l \hat{v}^m \hat{\theta}^n)_j} = \frac{2}{(2\pi)^{\frac{3}{2}}} \sum_{\substack{p,q,r=0 \\ l+p=\text{even}}}^{K \leqslant 4} \sigma_{v,j}^{m+q} \sigma_{\theta,j}^{n+r} C_{pqr} B_{l,p} B_{m,q} B_{n,r}, \tag{32}$$

$$\sigma_{v,j} = (1, -1, -1, 1), \quad \sigma_{\theta,j} = (1, 1, -1, -1). \tag{33}$$

As seen from these figures, the fractional contributions with $j = 1$ and 3 overwhelm those with $j = 2$ and 4, and thus the correspondence shown in figure 5 is almost completely satisfied. Hence, the structural models for $\overline{vv\theta}$ and $\overline{v\theta^2}$ can be written as

$$\overline{\hat{v}\hat{v}\hat{\theta}} \approx \overline{(\hat{v}\hat{v}\hat{\theta})_{j-1}} + \overline{(\hat{v}\hat{v}\hat{\theta})_{j-3}} = C[\sigma_{\overline{v\theta}} \tfrac{1}{2}\pi S(v) + S(\theta)], \tag{34}$$

$$\overline{\hat{v}\hat{\theta}^2} \approx \overline{(\hat{v}\hat{\theta}^2)_{j-1}} + \overline{(\hat{v}\hat{\theta}^2)_{j-3}} = C[S(v) + \sigma_{\overline{v\theta}} \tfrac{1}{2}\pi S(\theta)], \tag{35}$$

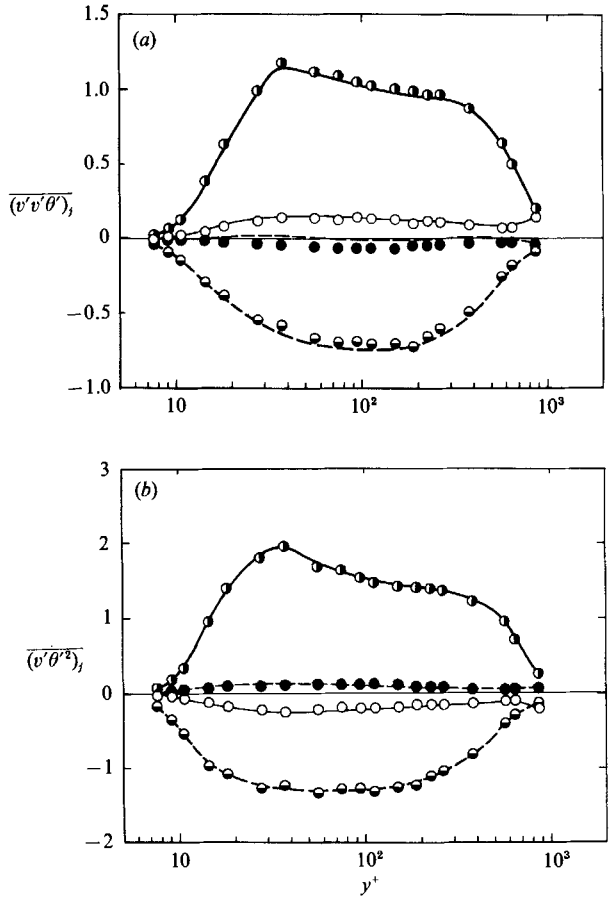

FIGURE 6. Fractional contributions of different events in the (v,θ)-plane to the third-order moments $\overline{vv\theta}$ and $\overline{v\theta^2}$. (*a*) $\overline{(vv\theta)_j}$, (*b*) $\overline{(v\theta^2)_j}$. Experiments: ◑, $j=1$; ○, $j=2$; ◒, $j=3$; ●, $j=4$. Calculations from (32): ——, $j=1$; ——, $j=2$; – – –, $j=3$; – – –, $j=4$.

where C is identical to (30) and $\sigma_{\overline{v\theta}}$ is defined by (31). Similarly, we can model $\overline{u^2\theta}$ and $\overline{u\theta^2}$.

On the other hand, if we model $\overline{vv\theta}$ on the basis of the fractional contributions in the (u,v)-plane (figure 3*b*), from (22) we obtain

$$\overline{\hat{v}\hat{v}\hat{\theta}} \approx \overline{(\hat{v}\hat{v}\hat{\theta})_{i-2}} + \overline{(\hat{v}\hat{v}\hat{\theta})_{i-4}} = \tfrac{1}{2}\overline{\hat{v}\hat{v}\hat{\theta}} - \frac{2}{\pi}\overline{\hat{v}\hat{u}\hat{\theta}}. \tag{36}$$

Rewriting (36) gives

$$\overline{\hat{v}\hat{u}\hat{\theta}} = \sigma_{uv}\tfrac{1}{4}\pi\,\overline{\hat{v}\hat{v}\hat{\theta}}. \tag{37}$$

Using (37) with (34) for $\overline{vv\theta}$, $\overline{vu\theta}$ can be predicted from the skewness factors $S(v)$ and $S(\theta)$.

5. Verification of structural models for triple products

The existence of structural similarity (Moin 1990) in shear-generated turbulence raises great expectations for the universality of the present structural models. In this section, we test the present structural models by application to various types of flows for which experimental results for triple products have been reported.

5.1. *Appraisal in velocity fields*

To assess the performance of the model, predictions for the following twelve test cases are shown in figures 7(*a–k*) and 8, and compared to the experimental data:

(*a*) pipe flow (Nagano & Tagawa 1988); figure 7(*a*)
(*b*) flat-plate boundary layer (Murlis, Tsai & Bradshaw 1982); figure 7(*b*)
(*c*) boundary layer on concave surface (Barlow & Johnston 1988); figure 7(*c*)
(*d*) boundary layer on concave surface (Shizawa & Honami 1986); figure 7(*d*)
(*e*) boundary layer on convex surface (Verriopoulos 1983); figure 7(*e*)
(*f*) asymmetric flow in a plane channel (Hanjalić & Launder 1972*a*); figure 7(*f*)
(*g*) conical diffuser flow (Azad & Ozimek 1986); figure 7(*g*)
(*h*) relaxing flat-plate boundary layer (Müller 1987); figure 7(*h*)
(*i*) wall jet (Irwin 1973); figure 7(*i*)
(*j*) two-dimensional mixing layer (Wygnanski & Fiedler 1970); figure 7(*j*)
(*k*) jet (Dekeyser & Launder 1985); figure 7(*k*)
(*l*) backward-facing step flow (Driver & Seegmiller 1985); figure 8.

Figure 7(*a–k*) shows that the present models (28) and (29) can satisfactorily reproduce the experiments not only in a qualitative sense but also quantitatively. Although the present structural models are established based essentially on the fact of wall turbulence, the high level of universality of the models is well worth noting. We believe that this indicates the existence of structural similarity in the generation process of the triple products in a variety of flows.

Figure 8 shows the comparison of predictions from (28) and (29) with measurements in a backward-facing step flow. Also included are those predicted from gradient-type diffusion models and those from a transport equation model (Amano & Chai 1988). A notable improvement upon the conventional models is seen in the transport model results of Amano & Chai (1988). However, the results for $y/H < 0.5$ are still unsatisfactory. On the other hand, the present structural model results agree well with the experiments.

5.2. *Appraisal in scalar fields*

The values of $\overline{vv\theta}$ and $\overline{v\theta^2}$ calculated from (34) and (35) and of $\overline{vu\theta}$ from (37) are shown in figures 9 and 10, respectively, which cover:

(*a*) heated pipe flow (Nagano & Tagawa 1988); figures 9(*a*) and 10
(*b*) heated boundary layer on convex surface (Verriopoulos 1983); figure 9(*b*).

Figure 9 shows that the structural model for $\overline{v\theta^2}$ reproduces the experiments as accurately as those for velocity fields. On the other hand, predictions of $\overline{vv\theta}$ are rather smaller than measurements. However, since there are few data available, we cannot discuss this problem further at the present stage.

Predictions of $\overline{vu\theta}$ are shown in figure 10, in which a dashed line represents the model results of (37) calculated using the experimental values of $\overline{vv\theta}$, and the solid line denotes those from (37) using (34). It appears that both lines well represent the experimental distribution.

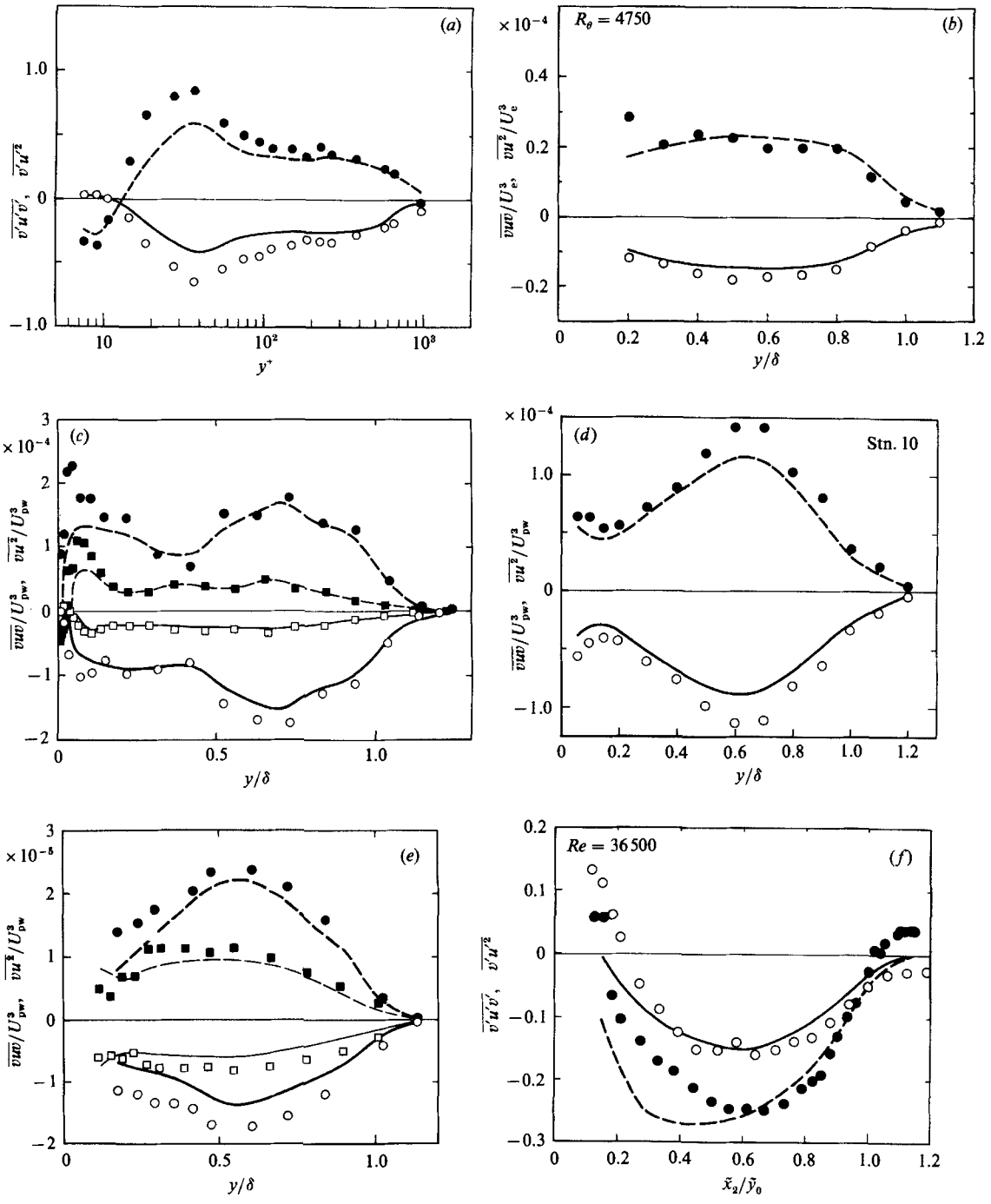

FIGURE 7. Tests of the structural models (28) and (29) in various types of flows. (*a*) Pipe flow (Nagano & Tagawa 1988). Experiments: ○, $\overline{vuv}$; ●, vu^2. Models results: ——, $\overline{vuv}$ predicted from (28); – – –, vu^2 predicted from (29). Measurement uncertainty at 95% coverage: ±20% for $\overline{vuv}$; ±18% for vu^2. (*b*) Flat-plate boundary layer (Murlis *et al.* 1982). Notation as in (*a*). (*c*) Boundary layer on concave surface (Barlow & Johnston 1988). Experiments on curved surface: ○, $\overline{vuv}$; ●, vu^2. Model results for curved surface: ——, $\overline{vuv}$; – – –, vu^2. Experiments on flat surface: □, $\overline{vuv}$; ■, vu^2. Model results for flat surface: ——, $\overline{vuv}$; – – –, vu^2. (*d*) Boundary layer on concave surface (Shizawa & Honami 1986). Notation as in (*a*). (*e*) Boundary layer on convex surface (Verriopoulos

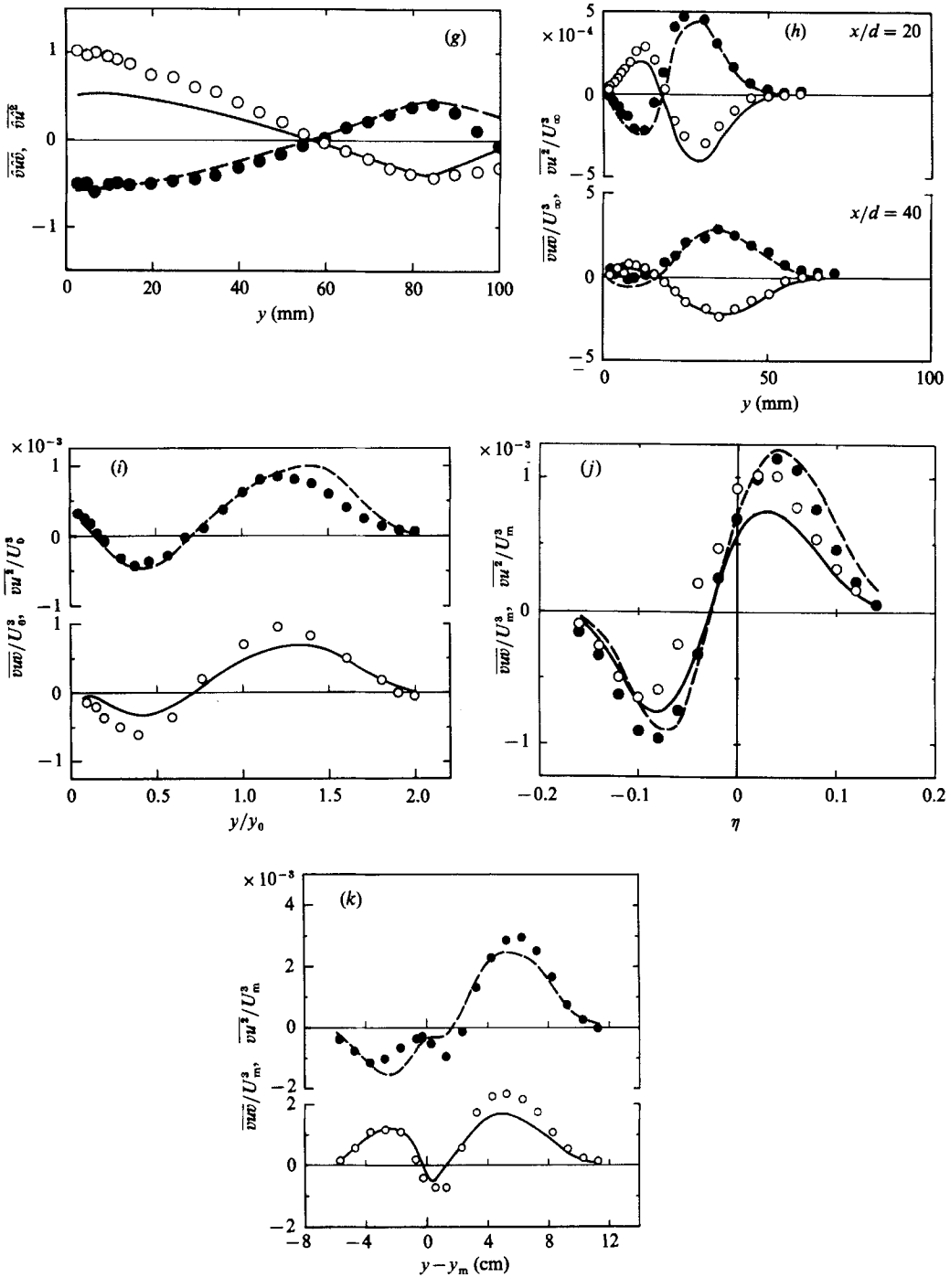

1983). Experiments on flat surface: ○, $\overline{vuv}$; ●, $\overline{vu^2}$. Model results for flat surface: ——, $\overline{vuv}$; – – –, $\overline{vu^2}$. Experiments on curved surface: □, $\overline{vuv}$; ■, $\overline{vu^2}$. Model results for curved surface: ——, $\overline{vuv}$; – – –, $\overline{vu^2}$. (*f*) Asymmetric flow in a plane channel (Hanjalić & Launder 1972*a*). Notation as in (*a*). (*g*) Conical diffuser flow (Azad & Ozimek 1986). Notation as in (*a*). (*h*) Relaxing flat-plate boundary layer (Müller 1987). Notation as in (*a*). (*i*) Wall jet (Irwin 1973). Notation as in (*a*). (*j*) Two-dimensional mixing layer (Wygnanski & Fiedler 1970). Notation as in (*a*). (*k*) Jet (Dekeyser & Launder 1985). Notation as in (*a*).

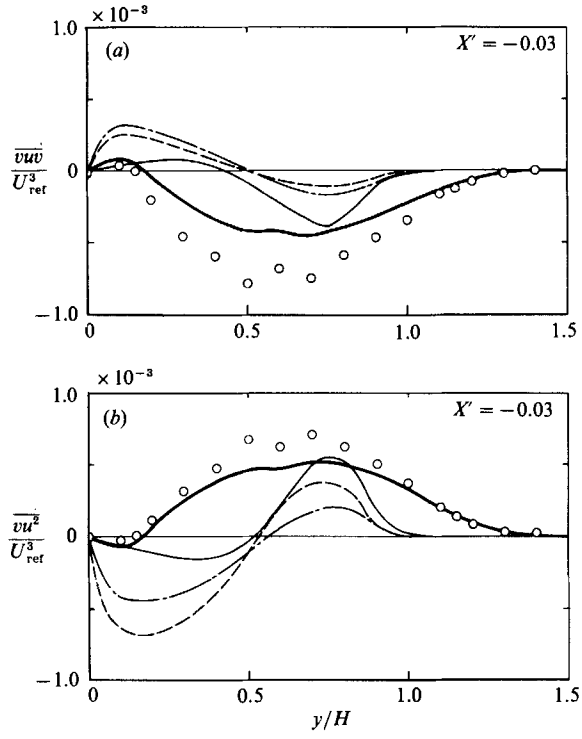

FIGURE 8. Comparison of model results for a backward-facing step flow. Model results: ——, present; ——, Amano & Chai (1988); – – –, Daly & Harlow (1970); — — —, Hanjalić & Launder (1972*b*). Experiments: ○, Driver & Seegmiller (1985). (*a*) $\overline{vuv}$; (*b*) $\overline{vu^2}$.

6. Usefulness of structural turbulence models for triple products

There are several particularly useful aspects of the present structural models for triple products.

When calculating triple products from their transport equations, we can substantially reduce the number of equations to be modelled. Thus, just $S(u)$, $S(v)$ and $S(\theta)$ are sufficient for representing $\overline{vuv}$, $\overline{vu^2}$, $\overline{vv\theta}$, $\overline{v\theta^2}$, $\overline{vu\theta}$, $\overline{u^2\theta}$ and $\overline{u\theta^2}$. But to obtain the skewness factors $S(u)$, $S(v)$ and $S(\theta)$, modelling the transport equation of a single component third-order moment $\overline{\chi^3}$ is required. However, this modelling is much simpler than that needed for general triple products $\overline{\chi_1\chi_2\chi_3}$ as described in Nagano & Tagawa (1990).

Also, we may simplify parameters characterizing triple products. For example, since the skewness factors $S(u)$ and $S(\theta)$ are nearly equal to zero in the log-law region of wall turbulence (Nagano & Tagawa 1988), we can see that $S(v)$ dominates the behaviour of other triple products. To cite another example, when the relation $S(u) = -S(v)$ holds as seen in a backward-facing step flow (Chandrsuda & Bradshaw 1981; Driver & Seegmiller 1985), other triple velocity products are represented by a single parameter $S(u)$ (or $S(v)$). Hence, we can see that a detailed investigation of $S(u)$ is most crucial in this case.

Finally, a cautionary note must be added. In the present structural models, the y-axis (with velocity component v) and the x-axis (with u) need to be fixed in the direction normal to the principal shear plane and parallel to it, respectively. Flow

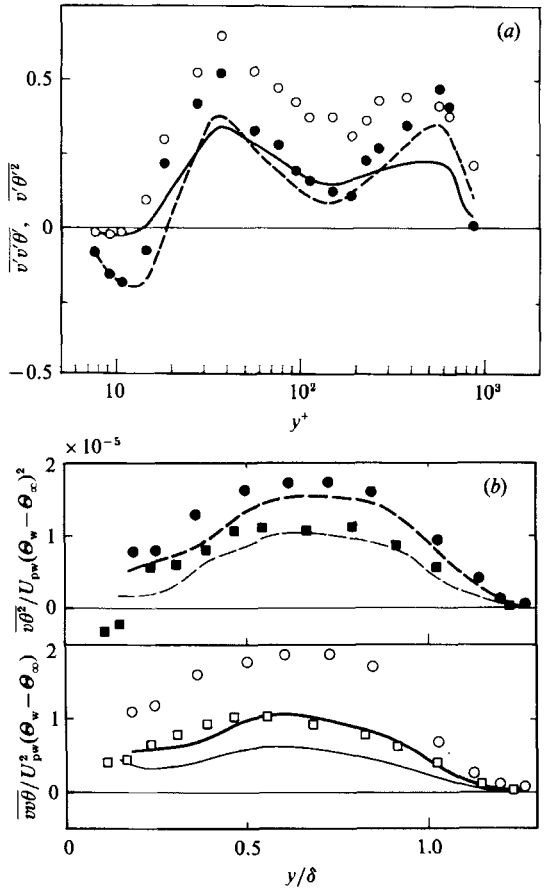

FIGURE 9. Tests of the structural models (34) and (35) in scalar fields. (*a*) Heated pipe flow (Nagano & Tagawa 1988). Experiments: ○, $\overline{vv\theta}$; ●, $\overline{v\theta^2}$. Models results: ——, $\overline{vv\theta}$ predicted from (34); – – –, $\overline{v\theta^2}$ predicted from (35). Measurement uncertainty at 95% coverage: ±20% for $\overline{vv\theta}$; ±18% for $\overline{v\theta^2}$. (*b*) Boundary layer on a heated convex surface (Verriopoulos 1983). Experiments on flat surface: ○, $\overline{vv\theta}$; ●, $\overline{v\theta^2}$. Model results for flat surface: ——, $\overline{vv\theta}$; – – –, $\overline{v\theta^2}$. Experiments on curved surface: □, $\overline{vv\theta}$; ■, $\overline{v\theta^2}$. Model results for curved surface: ——, $\overline{vv\theta}$; – – –, $\overline{v\theta^2}$.

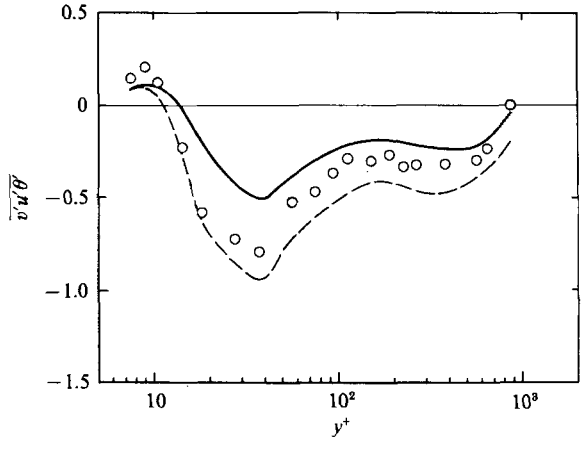

FIGURE 10. Test of the structural model for $\overline{vu\theta}$ (37) in a heated pipe flow (Nagano & Tagawa 1988). Experiment: ○. Model results: ——, predictions with (34) for $\overline{vv\theta}$; – – –, predictions with experimental values of $\overline{vv\theta}$. Measurement uncertainty at 95% coverage: ±18%.

analyses of importance in science and technology, however, are usually performed using such coordinate systems, and hence the present structural models may be used widely.

7. Conclusions

The statistical characteristics of third-order moments (triple products) in wall turbulence have been investigated from both experimental and theoretical points of view. On the basis of the results, we have made a new approach to the modelling of triple products of velocity and scalar needed in the Reynolds-stress and scalar-flux equation models. The results can be summarized as follows.

(i) The third-order moments in wall turbulence have a highly intermittent nature and are dominated almost completely by the coherent motions such as ejections and sweeps.

(ii) A very close similarity exists between the turbulent transport of the Reynolds shear stress $\overline{uv}$ and scalar flux $\overline{v\theta}$.

(iii) The structural turbulence models for triple products are constructed using physical behaviour of these quantities (equations (28), (29), (34), (35) and (37)). The models have simple forms and universal applicability, and their effectiveness has been tested by application to various types of flows.

REFERENCES

AMANO, R. S. & CHAI, J. C. 1988 Transport models of the turbulent velocity-temperature products for computations of recirculating flows. *Numer. Heat Transfer* **14**, 75–95.

AMANO, R. S., GOEL, P. & CHAI, J. C. 1988 Turbulence energy and diffusion transport of third-moments in a separating and reattaching flow. *AIAA J.* **26**, 273–282.

ANDRÉ, J. C., DE MOOR, G., LACARRÈRE, P., THERRY, G. & VACHAT, R. DU 1979 The clipping approximation and inhomogeneous turbulence simulations. In *Turbulent Shear Flows 1* (ed. F. Durst *et al.*), pp. 307–318. Springer.

ANSI/ASME PTC 19.1-1985 1986 *Measurement Uncertainty*. New York: ASME.

AZAD, R. S. & OZIMEK, L. G. 1986 A comparison of analog and digital systems of measurements of turbulence parameters. In *Proc. 10th Symp. on Turbulence*, pp. 27.1–27.10. University of Missouri-Rolla.

BARLOW, R. S. & JOHNSTON, J. P. 1988 Structure of a turbulent boundary layer on a concave surface. *J. Fluid Mech.* **191**, 137–176.

BENDAT, J. S. & PIERSOL, A. G. 1971 *Random Data: Analysis and Measurement Procedures*. John Wiley & Sons.

CHANDRSUDA, C. & BRADSHAW, P. 1981 Turbulence structure of a reattaching mixing layer. *J. Fluid Mech.* **110**, 171–194.

CORMACK, D. E., LEAL, L. G. & SEINFELD, J. H. 1978 An evaluation of mean Reynolds stress turbulence models: The triple velocity correlation. *Trans. ASME* I: *J. Fluids Engng* **100**, 47–54.

DALY, B. J. & HARLOW, F. H. 1970 Transport equations in turbulence. *Phys. Fluids* **13**, 2634–2649.

DEARDORFF, J. W. 1973 Three-dimensional numerical modeling of the planetary boundary layer. In *Proc. Workshop on Micrometeorology*, pp. 271–311. American Meteorological Society.

DEARDORFF, J. W. 1978 Closure of second- and third-moment rate equations for diffusion in homogeneous turbulence. *Phys. Fluids* **21**, 525–530.

DEKEYSER, I. & LAUNDER, B. E. 1985 A comparison of triple-moment temperature-velocity correlations in the asymmetric heated jet with alternative closure models. In *Turbulent Shear Flows 4* (ed. L. J. S. Bradbury *et al.*), pp. 102–117. Springer.

DONALDSON, C. DUP., SULLIVAN, R. D. & ROSENBAUM, H. 1972 A theoretical study of the generation of atmospheric-clear air turbulence. *AIAA J.* **10**, 162–170.

DRIVER, D. M. & SEEGMILLER, H. L. 1985 Features of a reattaching turbulent shear layer in divergent channel flow. *AIAA J.* **23**, 163–171.

DURST, F., JOVANOVIC, J. & KANEVCE, LJ. 1987 Probability density distribution in turbulent wall boundary-layer flows. In *Turbulent Shear Flows 5* (ed. F. Durst *et al.*), pp. 197–220. Springer.

HANJALIĆ, K. & LAUNDER, B. E. 1972*a* Fully developed asymmetric flow in a plane channel. *J. Fluid Mech.* **51**, 301–335.

HANJALIĆ, K. & LAUNDER, B. E. 1972*b* A Reynolds stress model of turbulence and its application to thin shear flows. *J. Fluid Mech.* **52**, 609–638.

IRWIN, H. P. A. H. 1973 Measurements in a self-preserving plane wall jet in a positive pressure gradient. *J. Fluid Mech.* **61**, 33–63.

LEE, M. J., KIM, J. & MOIN, P. 1987 Turbulence structure at high shear rate. In *Proc. 6th Symp. on Turbulent Shear Flows*, pp. 22.6.1–22.6.6. Toulouse.

LUMLEY, J. L. 1978 Computational modeling of turbulent flows. In *Advances in Applied Mechanics*, vol. 18 (ed. C.-S. Yih), pp. 123–176. Academic.

MOIN, P. 1990 Similarity of organized structures in turbulent shear flows. In *Near-Wall Turbulence* (ed. S. J. Kline & N. H. Afgan), pp. 2–6. Hemisphere.

MONIN, A. S. & YAGLOM, A. M. 1971 *Statistical Fluid Mechanics*, vol. 1, p. 233. MIT Press.

MÜLLER, U. R. 1987 The structure of turbulence measured in a relaxing boundary layer. In *Advances in Turbulence* (ed. G. Comte-Bellot & J. Mathieu), pp. 568–576. Springer.

MURLIS, J., TSAI, H. M. & BRADSHAW, P. 1982 The structure of turbulent boundary layers at low Reynolds numbers. *J. Fluid Mech.* **122**, 13–56.

NAGANO, Y. & HISHIDA, M. 1990 Turbulent heat transfer associated with coherent structures near the wall. In *Near-Wall Turbulence* (ed. S. J. Kline & N. H. Afgan), pp. 568–581. Hemisphere.

NAGANO, Y. & TAGAWA, M. 1988 Statistical characteristics of wall turbulence with a passive scalar. *J. Fluid Mech.* **196**, 157–185.

NAGANO, Y. & TAGAWA, M. 1990 Turbulence model for triple velocity and scalar correlations. In *Turbulent Shear Flows, 7* (ed. F. Durst *et al.*). Springer (to be published).

OWEN, R. G. 1973 An analytical turbulent transport model applied to non-isothermal fully-developed duct flows. Ph.D. Thesis, Pennsylvania State University.

SHIZAWA, T. & HONAMI, S. 1986 Experiments on turbulent boundary layers over a concave surface (2nd report, Response of turbulence to streamline curvature). *Trans. JSME* **52**, 2794–2801.

VERRIOPOULOS, C. A. 1983 Effects of convex surface curvature on heat transfer in turbulent flow. Ph.D. thesis, Imperial College.

WYGNANSKI, I. & FIEDLER, H. E. 1970 The two-dimensional mixing region. *J. Fluid Mech.* **41**, 327–361.

WYNGAARD, J. C. & COTÉ, O. R. 1974 The evolution of a convective planetary boundary layer: a higher-order-closure model study. *Boundary-Layer Met.* **7**, 289–308.

ZARIĆ, Z. 1979 Statistical evidence on the phenomena in wall layers of turbulent flows. In *Turbulent Forced Convection in Channels and Bundles*, vol. 1 (ed. S. Kakaç & D. B. Spalding), pp. 377–401. Hemisphere.